JOURNAL OF MATERIALS SCIENCE 31 (1996) 4333–4346

Growth kinetics of silver chloride precipitation in a Na_2O–B_2O_3 glass investigated by means of small-angle X-ray scattering and transmission electron microscopy

U. LEMBKE, K. GROSSE
Universität Rostock, Fachbereich Physik, Universitätsplatz 3, D-18051 Rostock, Germany

R. PASCOVA, I. GUTZOW
Institute of Physical Chemistry, Bulgarian Academy of Sciences, Acad. G. Bonchev str., bl. 11, Sofia 1040, Bulgaria

O. BECKER
Schott Glaswerke, Hattenbergstraße 10, D-55122 Mainz, Germany

L. HORN
Friedrich-Schiller-Universität Jena, Otto-Schott-Institut für Glaschemie, Fraunhoferstraße 6, D-07743 Jena, Germany

The kinetics of silver chloride cluster formation in a sodium borate glass heat treated isothermally at different temperatures above the glass transition temperature has been studied with small-angle X-ray scattering (SAXS). It is established that the size distributions of particle number and particle volume have bimodal shapes, i.e. the system of AgCl droplets consists of two populations with significantly different mean radii. The bimodality of the size distribution functions is confirmed by results of transmission electron microscopy (TEM) even if different techniques of sample preparation are used. The resolution limits of the TEM techniques applied amount to 2 nm and are comparable with the smallest particle diameters detectable by the SAXS method. The evolution of the size distributions is discussed in the framework of the theories of nucleation, growth and Ostwald ripening.

1. Introduction

The optical properties of photochromic glasses are determined by photosensitive crystallites consisting of silver halide which are dispersed in the glass. The kinetics of darkening and fading, the transmission and the colour of the darkened glass, and the wavelength of the activating radiation strongly depend on the composition of the microcrystalline halide phase and the conditions of the formation of the photosensitive particles as has been reported by Araujo [1, 2].

At the melting temperature the inorganic material forming the halide phase is dissolved in the glass melt. However, at intermediate temperatures close to the glass transition temperature T_g the glass is supersaturated with these substances and droplets of liquid silver halide can be precipitated by means of an appropriate heat treatment. During quenching of the heat-treated glass down to room temperature the droplets crystallize. It has been well known since the very beginning of the production of photochromic glasses by Armistead and Stookey [3–5] that the size distribution, the mean diameter, the number density and the volume fraction of the silver halide crystallites exert an important influence on the photochromic properties of the glass.

The formation mechanism of the photochromic silver chloride phase in a water soluble Na_2O–B_2O_3 model glass was investigated very thoroughly by Pascova and co-workers [6–8] using transmission electron microscopy (TEM), X-ray diffraction and nephelometric techniques. They extracted the phase diagram from solubility data obtained experimentally and showed that the silver halide separation from the glass may be described in terms of a binodal liquid–liquid phase separation and with the help of the classical theories of homogeneous nucleation and Ostwald ripening. The nucleation, growth and ripening of silver halide precipitates in commercial photochromic glasses has been studied by Lembke and co-workers [9–12] by means of small-angle X-ray scattering (SAXS). In contrast to the model glass of Pascova and co-workers in the commercial multicomponent photochromic glasses, which contained much smaller amounts of silver halide than the aforementioned sodium borate model glass, heterogeneous nucleation was found to be the dominant

0022–2461

mechanism of nucleation. The results of the SAXS experiments suggested a bimodal-type silver halide size distribution, i.e. the existence of two distinct maxima, even in the early stages of ripening.

A similar result of a size distribution with two maxima was obtained by investigating the water soluble Na_2O–B_2O_3 photochromic model glass [6–8] with SAXS techniques. In [13] these experimental data were discussed based on a theoretical model computation which allows one to calculate the expected size distribution under different conditions for a given set of thermodynamic parameters of the glass. The analysis based on homogeneous nucleation showed that, assuming growth by attachment of single monomers and non-overlapping diffusion zones of the forming particles, bimodal-type size distributions can only be obtained if either a prepopulation of small clusters exists, which is produced during quenching the liquid melt to glass and has initial particle dimensions below the resolution limit of the experiment, or if a size-dependent diffusion coefficient in consequence of elastic strain effects is considered [13].

Up to now the existence of bimodal size distributions of microcrystallites in photochromic glasses has been established only by the SAXS method. Therefore, the aim of the present paper is a comprehensive experimental investigation of the phenomenon of bimodal size distributions with significantly different mean radii of the two cluster populations. The SAXS results are proved by TEM applying appropriate preparation techniques.

2. Experimental methods

2.1. Preparation of the glass

The model glass was prepared in a platinum crucible at 1000 °C from the reagent grade raw materials, boric acid and borax containing a small amount of CuO and 4.5 wt % AgCl. The glass melt of the composition 29.31 Na_2O–68.38 B_2O_3–2.17 AgCl–0.14 CuO (mol %) was poured onto a cold stainless steel plate and pressed quickly by another stainless steel plate resulting in cooling rates of approximately 500 Ks^{-1}. This quenching procedure was necessary in order to avoid the nuclei formation of the AgCl phase during cooling of the melt down to room temperature. The glass platelets obtained with dimensions of about $20 \times 10 \times 0.5\ mm^3$ were heat treated under isothermal conditions at $T = 466$ °C and $T = 480$ °C for different treatment times.

2.2. Small-angle X-ray scattering (SAXS)

SAXS is a diffraction method that permits one to obtain structure information in the size range typical of colloidal dimensions, i.e. in general from 1 up to 200 nm. Owing to spatial fluctuations of the electron density in the sample the interference of scattered X-rays produces a scattering pattern surrounding the primary beam in the region of very small scattering angles θ or small values of the modulus s of the scattering vector,

$$s = 4\pi \sin(\theta/2)/\lambda \quad (1)$$

where λ is the X-ray wavelength. For example, the development of the SAXS intensities during the heat treatment of the glass at $T = 480$ °C is shown in Fig. 1. The scattering curves $\tilde{I}(s)$ were measured with a Kratky camera using "infinitely long" slit collimation [14], step scanning, CuK_α radiation filtered by a nickel foil, and an X-ray proportional counter with single-channel analyser.

The absolute scattering intensity $\tilde{I}(s)$, i.e. normalized to the scattering intensity of a single electron with the help of a Lupolen® standard sample, is the Fourier transform of the correlation function $C(r)$ which contains all structure information about the spatial arrangement of the excess electron density $\Delta\rho_e(r)$ in the sample [16]:

$$C(r) = \langle \Delta\rho_e(r')\Delta\rho_e(r'+r) \rangle \quad (2)$$

The correlation function is calculated from $\tilde{I}(s)$ according to [18]

$$C(r) = 1/(4\pi^2)\int_0^\infty sJ_0(sr)\tilde{I}(s)\mathrm{d}s \quad (3)$$

J_0 is the zero-order Bessel function of the first kind. For homogeneous spheres dispersed in a dilute system, i.e. neglecting interparticle interference and multiple scattering effects, the particle diameter distribution function $N^*(D)$ is defined as follows [17]:

$$\frac{\mathrm{d}N^*(D)}{\mathrm{d}D} - \frac{\mathrm{d}}{\mathrm{d}r}\left[\frac{\mathrm{d}^2C(r)}{\mathrm{d}r^2}\right]_{r=D} \quad (4)$$

D is the diameter of the spherical particle. $C(r)$ and $N^*(D)$ can be calculated directly from the slit-smeared scattering curves $\tilde{I}(k\Delta s)$ by series expressions applying a transform technique which is based on the sampling theorem of the information theory [18]. The scattering curve detected in a limited sector of the scattering angle at distinct points k with the increment Δs has to be extrapolated to $\tilde{I}(0)$ according to Guinier's law [15] and to infinity corresponding to Porod's law [19].

In the present case of a two-phase system consisting of the small AgCl droplets and the glass matrix, the volume fraction w of the silver halide phase can be determined from the value of the correlation function $C(r)$ for $r = 0$,

$$C(0) = 1/(4\pi^2)\int_0^\infty s\tilde{I}(s)\,\mathrm{d}s = \langle(\Delta\rho_e)^2\rangle \quad (5)$$

because for two-phase systems the following expression for the mean squared electron density fluctuation $\langle(\Delta\rho_e)^2\rangle$ is valid:

$$\langle(\Delta\rho_e)^2\rangle = w(1-w)(\Delta\rho_e)^2 \quad (6)$$

The difference $\Delta\rho_e$ between the electron densities of the AgCl particles and the glass matrix can be calculated from the compositions of the phases given in the phase diagram determined in [6].

Taking into account that the integrated volume of all individual particles dispersed within a unit volume

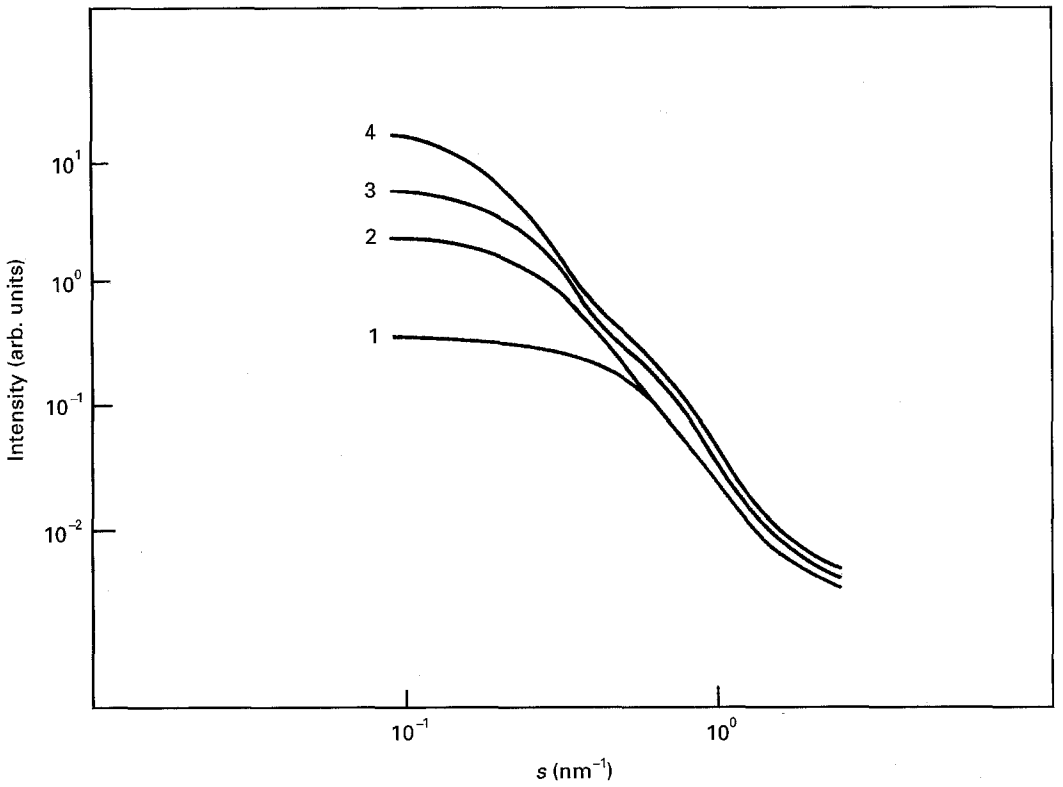

Figure 1 Small-angle X-ray scattering (SAXS) curves registered for the glass samples heat treated at $T = 466\,^{\circ}C$; double-logarithmic scales. Key: 1, 15 min; 2, 30 min; 3, 60 min; 4, 120 min.

of the sample is equal to the AgCl volume fraction w the computed size distribution $dN^*(D)/dD$ is normalized:

$$\frac{dN(D)}{dD} = w\frac{dN^*(D)}{dD}\Big/\left[(\pi/6)\int_0^\infty\left(D^3\frac{dN^*(D)}{dD}\right)dD\right] \quad (7)$$

That means that the number density N_v of the AgCl particles in the sample is represented by the area under the particle diameter distribution function $dN(D)/dD$:

$$N_v = \int_0^\infty dN(D) \quad (8)$$

Consequently, the volume distribution function

$$\frac{dw}{dD} = (\pi/6)\,D^3\frac{dN(D)}{d(D)} \quad (9)$$

defines that fraction of the phase volume w to which all AgCl crystallites with a diameter between D and $D + dD$ contribute.

It has to be mentioned, however, that owing to the limited sector of the scattering angle, where SAXS can be detected, the structure data may be discussed only within a limited region of r or D. The resolution limit of the experimental data presented is $D_{min} = 2$ nm and the largest particles covered by our SAXS experiments have a diameter $D_{max} = 40$ nm. This must be taken into account if the SAXS results are compared with the outcomes of another method.

2.3. Transmission electron microscopy

2.3.1. Pt/C replica of the fractured glass

The photochromic sodium borate model glass was fractured in vacuum. Remaining in the vacuum chamber the as-fractured surface was immediately covered by a thin film of evaporated platinum and carbon (shadowing under 45°). The Pt/C film was peeled off from the glass with 1N HNO_3. After washing with distilled water the replica was examined in the electron microscope. The amplification factor of the TEM micrograph taken from the film was calibrated with the help of a Ludox standard. Considering the inhomogeneity of the investigated Pt/C films the resolution limit for the detection of silver halide microcrystallites is about 15 nm (see Fig. 2).

2.3.2. Centrifuged aqueous solutions of the glass

The water solubility of the selected matrix glass offered the possibility to investigate the morphology and the size distribution of the AgCl phase by a very original method. For this purpose a small sample of the heat treated model glass (about 20 mg) was dissolved in water. The AgCl crystallites thus extracted from the matrix glass were centrifuged with a speed of 11000 r.p.m. onto a Formvar layer. The layer was investigated with TEM; a typical micrograph is shown in Fig. 3. The resolution limit obtained is about 2 nm. The dissolution of glass samples for TEM investigations was carried out in water previously saturated with AgCl containing 4.6×10^{-5} moll^{-1} K-eosine. According to [20] K-eosine inhibits the growth and dissolution of the AgCl crystallites as-extracted from the glass matrix in water. This property of K-eosine was proven in a previous publication [7]. The inhibition effect of K-eosine is maintained up to a certain critical concentration c_c of AgCl as has been shown by

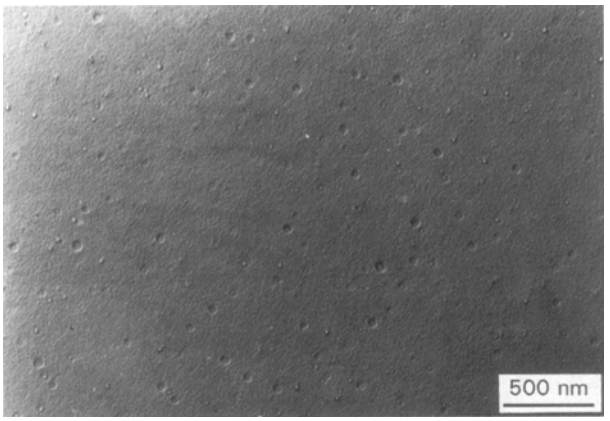

Figure 2 TEM micrograph of AgCl microcrystallites dispersed in the glass matrix obtained by Pt–C replica from the surface of the sample fractured under vacuum and treated at $T = 480\,°C$ for $t = 180$ min.

nephelometric measurements of aqueous solutions of the model glass [6, 8]. This critical concentration was taken into account when the AgCl crystallites were extracted from the model glass. Consequently, the dissolution of the glass sample was carried out under circumstances which guaranteed the preservation of the primary morphology and size distribution of the AgCl crystallites precipitated in the glass.

2.3.3. Preparation by ion sputtering and ultramicrotomy

Prior to the ion beam etching small glass platelets were prepared by grinding and polishing. The 100 μm thick samples were thinned down to 15 μm in the centre applying a dimple grinder and 3 μm diamond powder. After polishing with 1 μm CeO_2 powder and cleaning with methanol the samples were thinned by ion sputtering the glass. A focused beam of Ar^+ ions

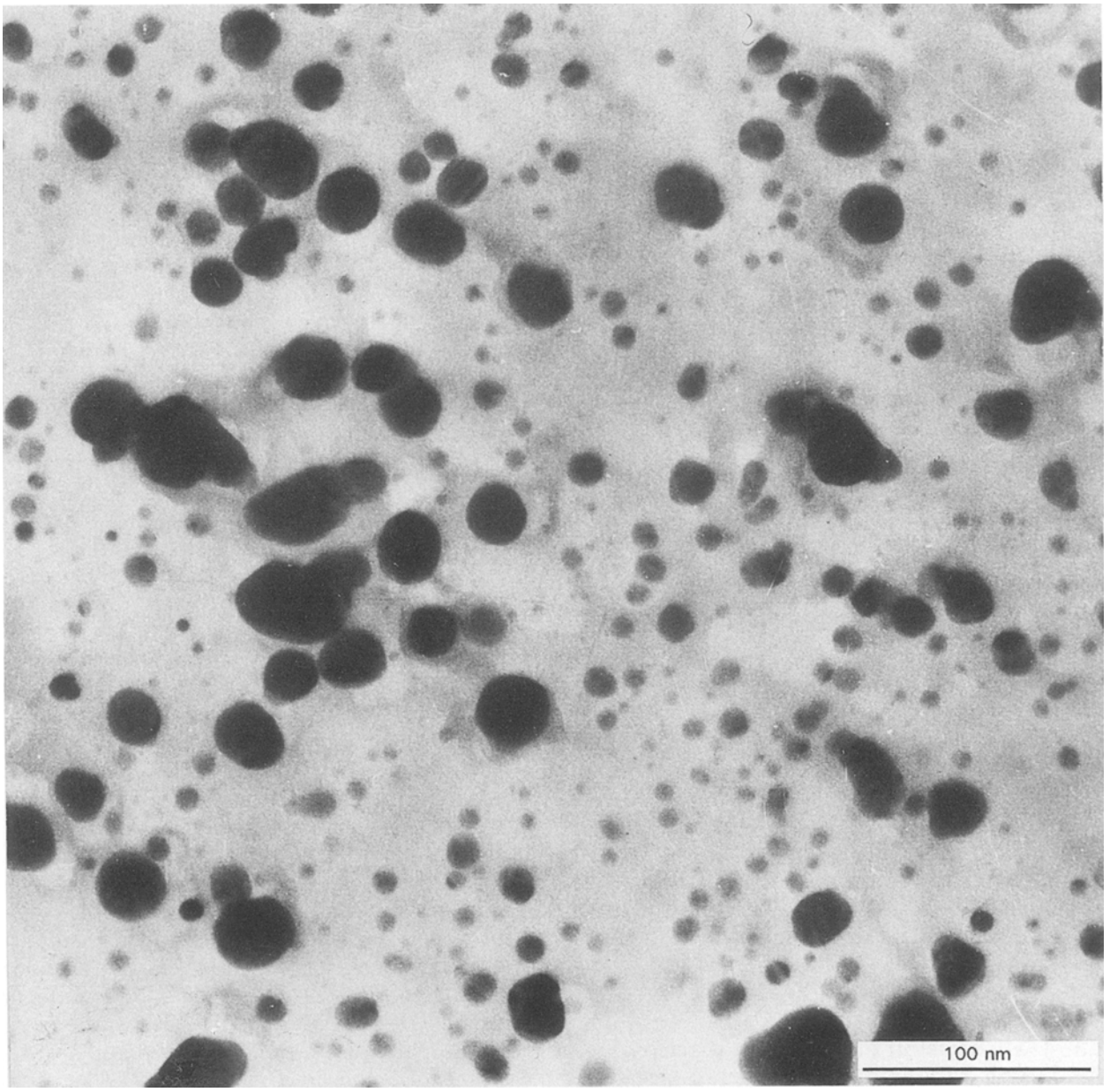

Figure 3 TEM micrograph of the AgCl particles dispersed in the sample treated at $T = 480\,°C$, $t = 180$ min, obtained after dissolving the glass in water and after centrifuging the particles onto Formvar layers.

(6 KeV, $I = 0.2\ \mu A\ mm^{-2}$) etched the sample down to the thickness necessary for electron transparency [21]. The edges of the etched holes were investigated by TEM. Particles with diameters of about 2 nm are easily resolved.

In order to avoid structural changes within the sample which could be initiated by ion beam etching in addition to the other TEM preparation techniques ultramicrotome cutting was carried out. According to the method described in [22–24] a small strip of the glass is imbedded in a resin block which is ground to a truncated pyramidal shape. From the top of the truncated pyramid, an area of about $0.3 \times 1\ mm^2$, thin sections were obtained by cutting the sample with a diamond knife whilst clamped in a specimen holder. The 50 nm thick glass sections floated onto the surface of water in a trough behind the knife edge and were picked up on the electron-microscope sample holder. For hygroscopic samples the cutting procedure can also be performed without water, as was done in the present case for confirmation.

3. Results

From the SAXS curves measured for different isothermal heat treatments (see, for example, Fig. 1) the silver chloride volume fractions w were obtained by performing the calculation according to Equations 5 and 6. The contrast of the electron density was computed using the molar weights of the glass components, the macroscopic glass density and the bulk electron density of AgCl, respectively: $\rho_{e,glass} = 6.86 \times 10^{23}\ cm^{-3}$, $\rho_{e,AgCl} = 14.96 \times 10^{23}\ cm^{-3}$ and, therefore, $(\Delta\rho_e)^2 = 6.56 \times 10^{47}\ cm^{-6}$. The evolution of w during the heat treatment is shown in Fig. 4. The saturation value for long treatment durations $w_{max} = 1.4\%$, representing the maximum phase volume of precipitated AgCl, is approximately the same for both treatment temperatures. In the case of $T = 466\,°C$ this value is reached later than for the temperature of $T = 480\,°C$ as is expected because of the lower diffusion mobility at the lower temperature. The behaviour of $w(t)$ in Fig. 4 points out that our investigation covers the stages of particle growth and the beginning of ripening of the phase separation of silver chloride in the sodium borate glass.

Coarsening by ripening starts if the supersaturation of the glass with silver halide monomers is almost zero. Consequently, a constant phase volume is expected for the ripening stage (Fig. 4). Furthermore, in consequence of the dissolution of small particles and further growth of large particles the number of halide droplets decreases. This behaviour is well illustrated in Fig. 5, where the particle number densities N_V obtained by Equation 8 are drawn versus treatment time t. Obviously, at $T = 480\,°C$ the process of Ostwald ripening has already started during the first 15 min of the heat treatment. Corresponding to the so-called LSW theory of ripening developed by Lifshitz and Slyozov [25] and Wagner [26], in the asymptotic stage of diffusion-limited ripening, a power law of $N_V(t) \sim t^{-1}$ can be observed owing to the competing growth of dissolving small particles and growing large clusters. At $T = 466\,°C$ the number of dispersed AgCl droplets initially even increases indicating nucleation and growth of newly formed particles until for $t \geqslant 60$ min ripening starts to become the dominant growth mechanism.

Nucleation, growth and ripening can also be characterized by studying the evolution of the size

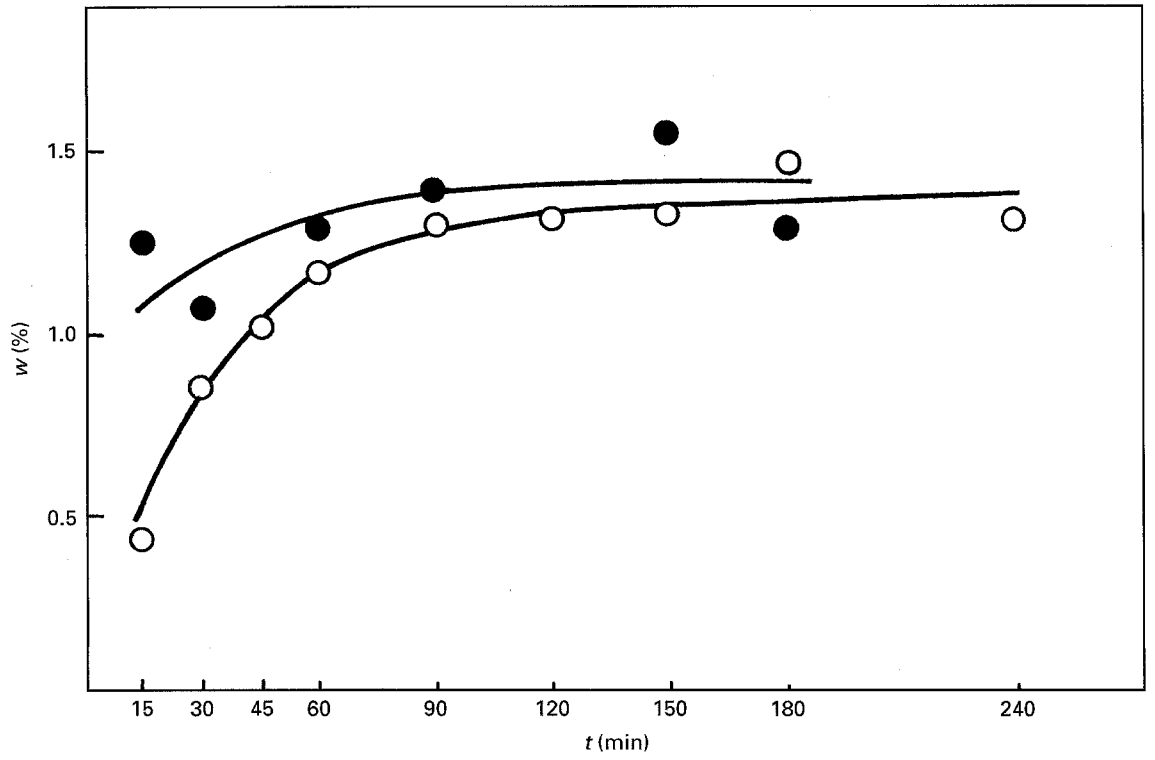

Figure 4 Evolution of the AgCl volume fraction $w(t)$ during the heat treatment at two different temperatures; t is the time of isothermal treatment. Key: ● $T = 480\,°C$; ○ $T = 466\,°C$.

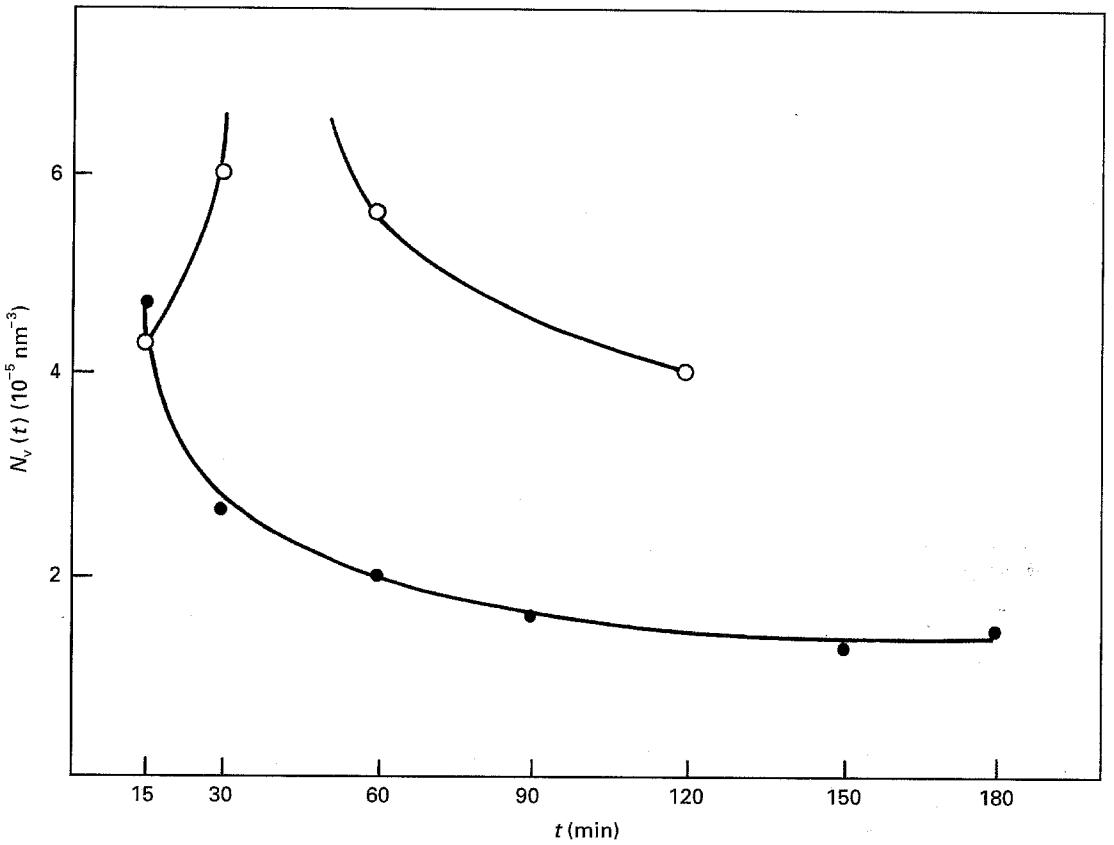

Figure 5 Development of the number density $N_V(t)$ of the AgCl microcrystallites depending on the treatment time t. Key: ● $T = 480\,°C$; ○$T = 466\,°C$.

distribution and the volume distribution. These structure functions are obtained from the recorded SAXS data following Equations 4–7 and 9. The particle size distributions, which are defined, in the mathematical sense, to be density distribution functions, are shown for different treatment conditions in Figs 6a and 7a. These distributions point out that a population of very small particles exists with diameters which are close to the resolution limit of the SAXS experiment (2 nm). The number of small particles exceeds by about three orders of magnitude the number of larger clusters. The tail region almost disappearing in the linear plot representing larger particles (see the insets in Figs 6a and 7a), which are dominated in the particle density N_V by the small clusters but form the main part of the AgCl phase volume, can be better observed in the volume distributions dw/dD calculated according to Equation 9 and these are shown in the Figs 6b and 7b. Here, the bimodal-type size distributions, i.e. the existence of two distinct populations of clusters which grow and ripen and have different mean diameters, are evidently demonstrated.

This experimental result already described in [9–12] for commercial photochromic glasses was verified for the present glass system with the help of electron microscopy. Fig. 2 shows the TEM micrograph of a Pt–C replica from the surface of the sample fractured under vacuum and heat treated at $T = 480\,°C$ for $t = 180$ min. Using a reader for microfilms (overall amplification of TEM micrograph and reader: 1.85×10^8) a histogram was obtained from the photographic plates. This histogram is marked by a dashed line in Fig. 8. Owing to the structure of the Pt–C layer the resolution limit is about 15 nm. Consequently, we were not able to detect most of the particles that should belong to the smallest diameter grade in the dashed histogram of Fig. 8.

Another problem with the quantitative analysis of the micrographs from the fractured glass surfaces is illustrated by the inset in Fig. 8. The majority of the crystallites in the matrix glass are not fractured along the equator planes that reflect the real diameters but frequently the fracture planes suggest apparently smaller particle dimensions. Considering this effect the apparent diameter histogram $n(D)$ (dashed curve in Fig. 8) must be corrected in order to calculate the real histogram. Following the approach in [27], in the case of spherical particles the probability that a droplet with the diameter D is fractured and that the fracture plane has a diameter $\leqslant d$ amounts to

$$P(D, d) = 1/D_{max}[D - (D^2 - d^2)^{1/2}] \quad (10)$$

where D_{max} is the diameter of the largest particle contained in the volume. Therefore, for a histogram consisting of i_{max} size grades with a maximum diameter D_i of the respective size grade i Equation 10 becomes:

$$P(D_i, D_{j\leqslant i}) = 1/D_{max}[D_i - (D_i^2 - D_j^2)^{1/2}] \quad (11)$$

Accordingly, the probability that a particle having a real diameter D within the size grade i, i.e. $D_{i-1} < D \leqslant D_i$, is fractured and registered in such a manner that it is classified into its correct size grade

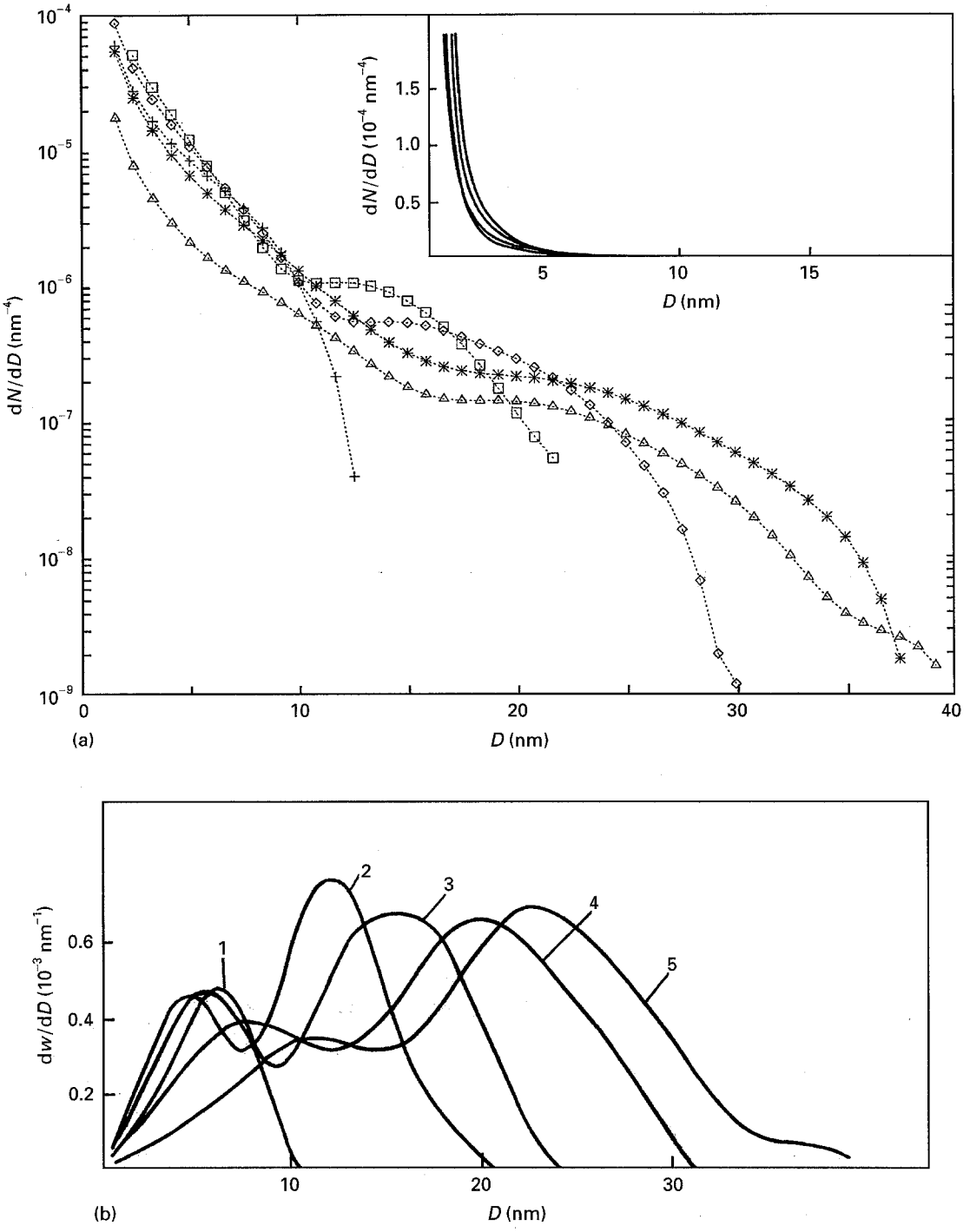

Figure 6 (a) The particle size distributions obtained from the SAXS data; treatment at $T = 466\,^{\circ}C$. The axis of dN/dD is given as a logarithmic scale in order to emphasize the bimodal character of the size distributions which can not be evaluated in a linear plot (see the inset). Key: --- +--- 15 min; ---□--- 30 min; ---◇--- 60 min; --- ✳ --- 120 min; ---△--- 240 min; (b) The volume distribution functions corresponding to the size distributions in (a). Key: 1, 15 min; 2, 30 min; 3, 60 min; 4, 120 min; 5, 240 min.

i is

$$P_{i,i} = 1 - P(D_i, D_{i-1})$$
$$= 1/D_{max}[D_{max} - D_i + (D_i^2 - D_{i-1}^2)^{1/2}] \quad (12)$$

That fraction of particles with the real size grade $i + j$ that has been allocated to grade i owing to a fracture plane smaller than the particle diameter is described by

$$P_{i+j,i} = P(D_{i+j}, D_i) - P(D_{i+j}, D_{i-1})$$
$$= 1/D_{max}[(D_{i+j}^2 - D_{i-1}^2)^{1/2} - (D_{i+j}^2 - D_i^2)^{1/2}]$$
$$\text{for } i < i + j \leqslant i_{max} \quad (13)$$

Based on the Equations 12 and 13 the measured histogram can be corrected by means of a recursion formalism. Due to the absence of particles larger than D_{max} the number of particles $n_{i\,max}$ registered in the largest size grade i_{max} is equal to the fraction $P_{i\,max,i\,max}$ of the real particle number $N_{i\,max}$ in grade i_{max} according to Equation 12. Therefore, the corrected number in the largest grade is obtained using

$$N_{i\,max} = n_{i\,max}/P_{i\,max,i\,max} \quad (14)$$

The particle numbers in the other size grades are corrected consecutively starting with $i = i_{max} - 1$ and

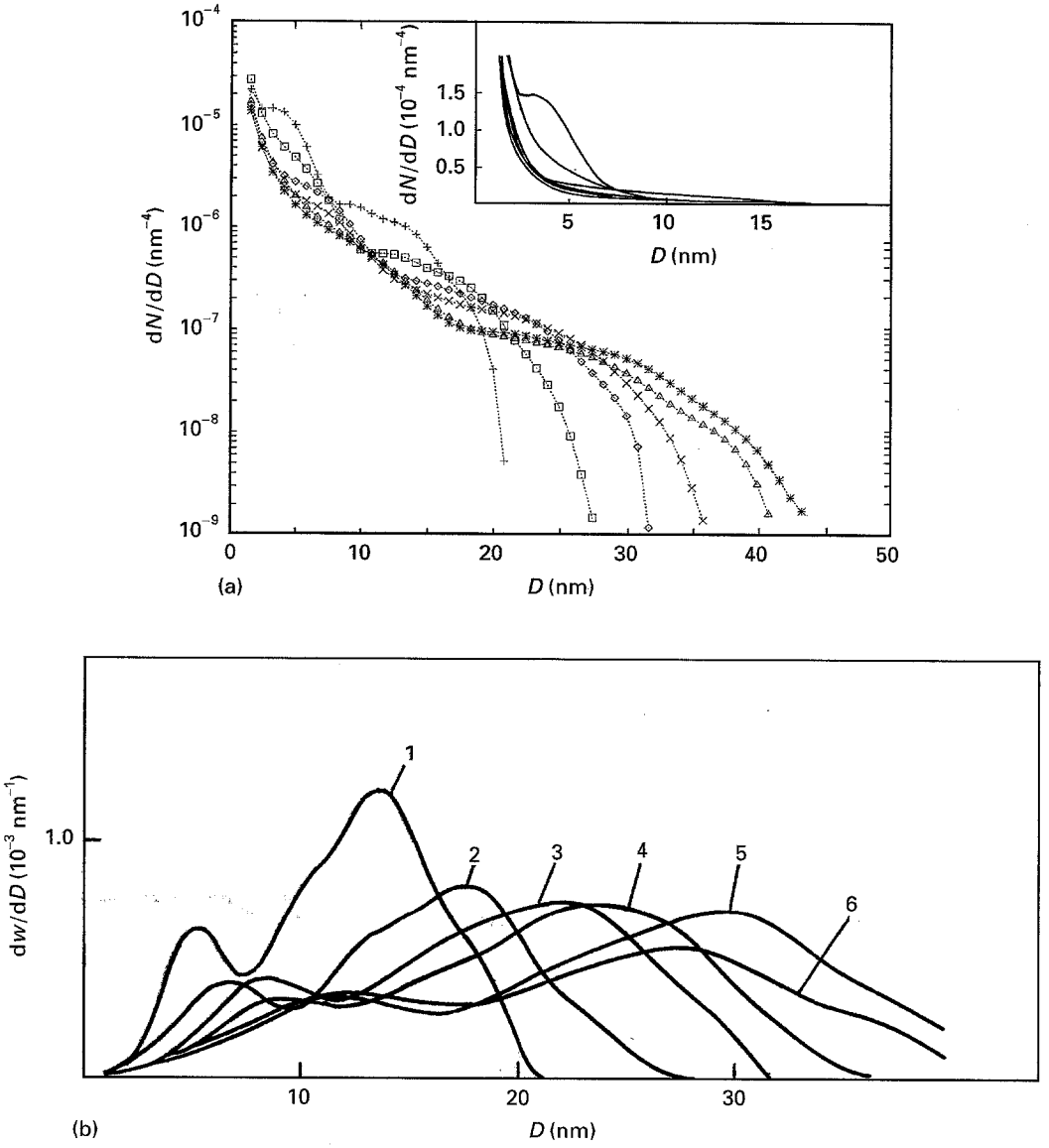

Figure 7 (a) The particle size distributions obtained by SAXS, treatment at $T = 480\,^{\circ}C$. The axis of dN/dD is given as a logarithmic scale; inset: linear scales. Key: --- +--- 15 min; ---□--- 30 min; ---◇--- 60 min; ---×--- 90 min; --- ✳ --- 150 min; ---△--- 180 min. (b) Development of the volume distribution function at $T = 480\,^{\circ}C$. Key: 1, 15 min; 2, 30 min; 3, 60 min; 4, 90 min; 5, 150 min; 6, 180 min.

decreasing i step by step. The real particle number N_i,

$$N_i = \left(n_i - \sum_{j=1}^{i_{max}-1} N_{i+j}P_{i+j,i}\right)/P_{i,i} \quad \text{for } i < i_{max} \quad (15)$$

is obtained by subtracting the sum of the fractions of the larger particles, which have been attributed to grade i but belong to their real grade $i + j$, from the number n_i of the fracture planes recorded in grade i and dividing this number of particles having the real dimension of grade i by the corresponding detection probability $P_{i,i}$.

Applying the above mentioned correction technique to the registered histogram $n(D)$, the real histogram $N(D)$ characterizing the true size distribution of AgCl microcrystallites in the glass can be extracted. $N(D)$ is drawn with a solid line in Fig. 8. Obviously, this diagram confirms qualitatively the abundance of small particles in relation to the few larger clusters. On the other hand the result shown in Fig. 8 can barely be regarded as convincing proof for the bimodality of the size distribution established by SAXS. The limited size resolution of the TEM micrograph taken from a Pt/C replica and the statistical uncertainty of the size histogram obtained restrict the significance of the findings.

The experimental advantage of a water soluble matrix glass offers the opportunity for another TEM preparation technique. As described in section 2.3.2 the AgCl microcrystallites were extracted from aqueous solutions of the glass by a centrifuge. A typical detail of the TEM picture taken from the centrifuged AgCl precipitates of the sample heat treated at $T = 480\,^{\circ}C$, $t = 180$ min, is presented in Fig. 3. The corresponding histogram of the silver halide microcrystallites averaged over 616 particles is shown in Fig. 9. In consequence of the high speed of the centrifuge and the high resolution of the electron microscope used the resolution limit of this experiment is 2.5 nm. Differentiating this histogram and normalizing the total volume of the particles to the phase volume w determined by SAXS the size distribution in Fig. 10 and the corresponding volume distribution in Fig. 11 are obtained. These TEM results are very

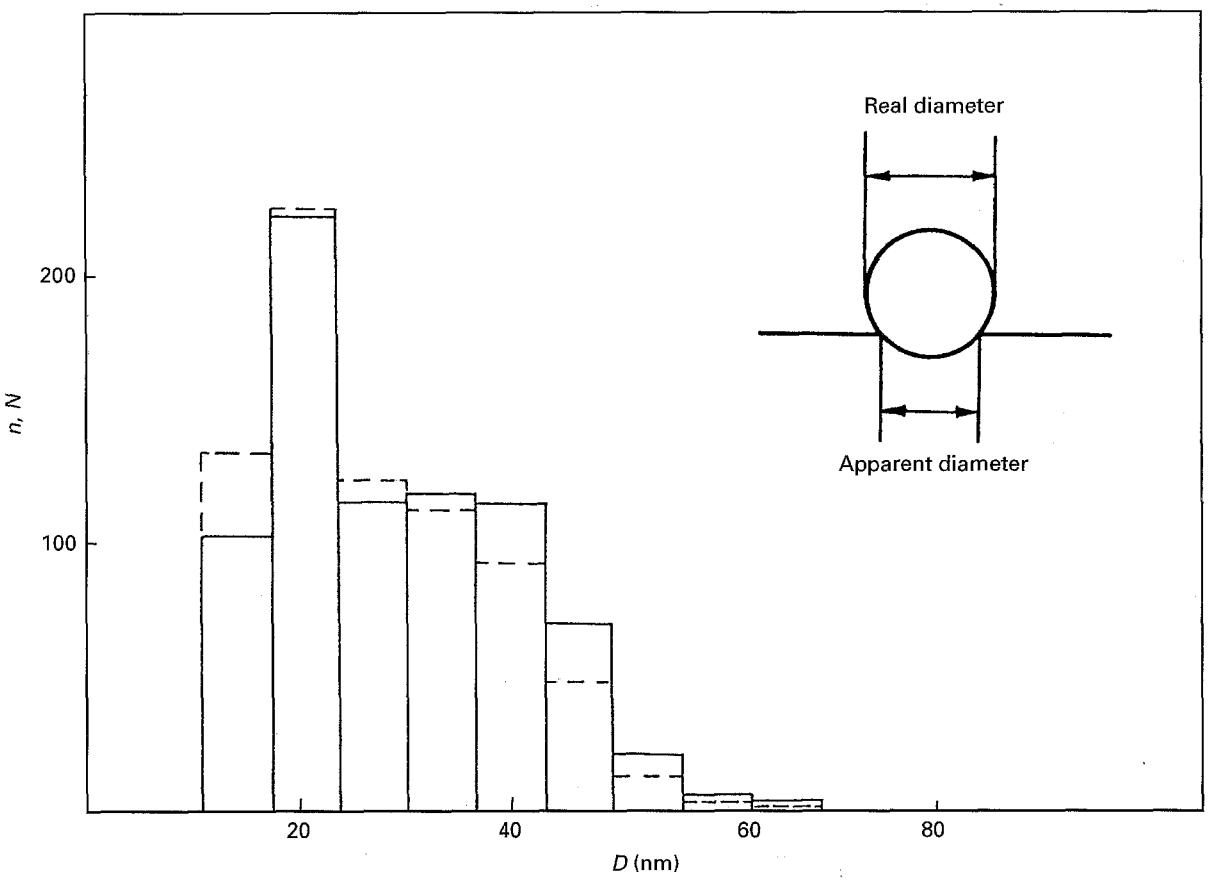

Figure 8 Histogram of the AgCl crystallite dimensions resulting from the TEM micrograph shown in Fig. 2: particle numbers n and N versus particle diameter D. The as-recorded histogram $n(D)$ (dashed line) representing the distribution of the apparent particle diameters registered on the TEM micrograph of the Pt–C replica was corrected according to Equations 10–15 in order to obtain the histogram of the real particle diameters $N(D)$ (solid line). The methodical problem of this conventional preparation technique for TEM is illustrated schematically in the inset.

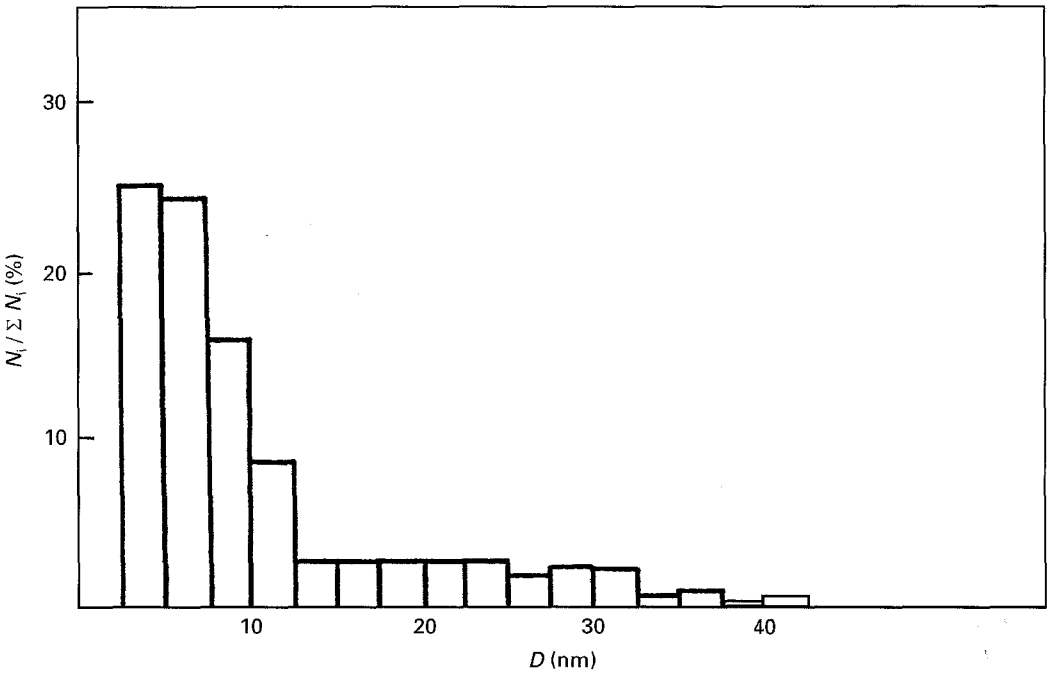

Figure 9. Size histogram obtained by evaluating the TEM micrograph shown in Fig. 3: particle numbers N_i of different size grades i normalized to the total number of particles registered versus crystallite diameter D; sample: $T = 480\,^{\circ}C$, $t = 180$ min.

similar to those of the SAXS experiments. A large number of small particles is detected and a long tail of only a few larger particles is observed in the size distribution. The TEM volume distribution turns out to be bimodal and, therefore, the shape of the AgCl particle size distributions determined by SAXS is confirmed.

In order to receive additional experimental evidence for these results TEM micrographs were taken from heat treated glass samples thinned by ion sputtering

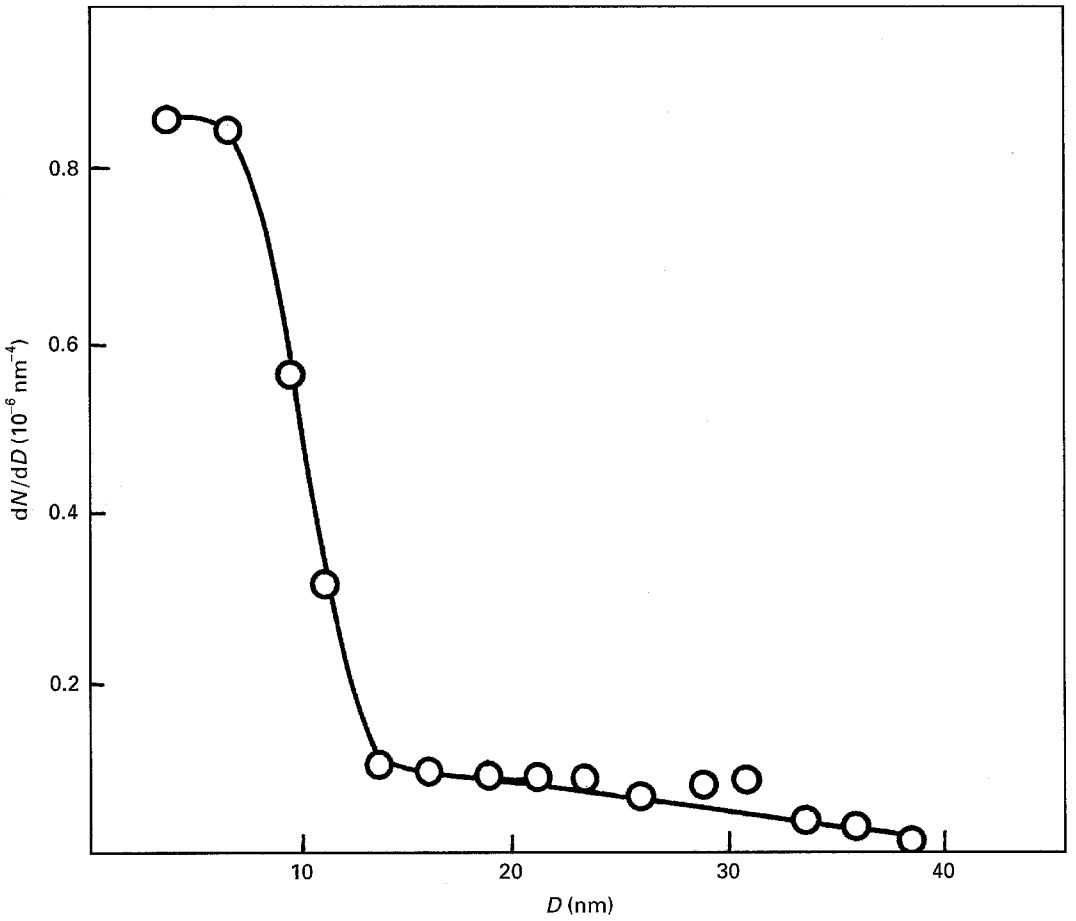

Figure 10 The size distribution obtained from the histogram Fig. 9 and normalized in such a manner that the total volume of all particles is equal to the phase volume $w = 1.4\%$ calculated by means of SAXS (see Fig. 4).

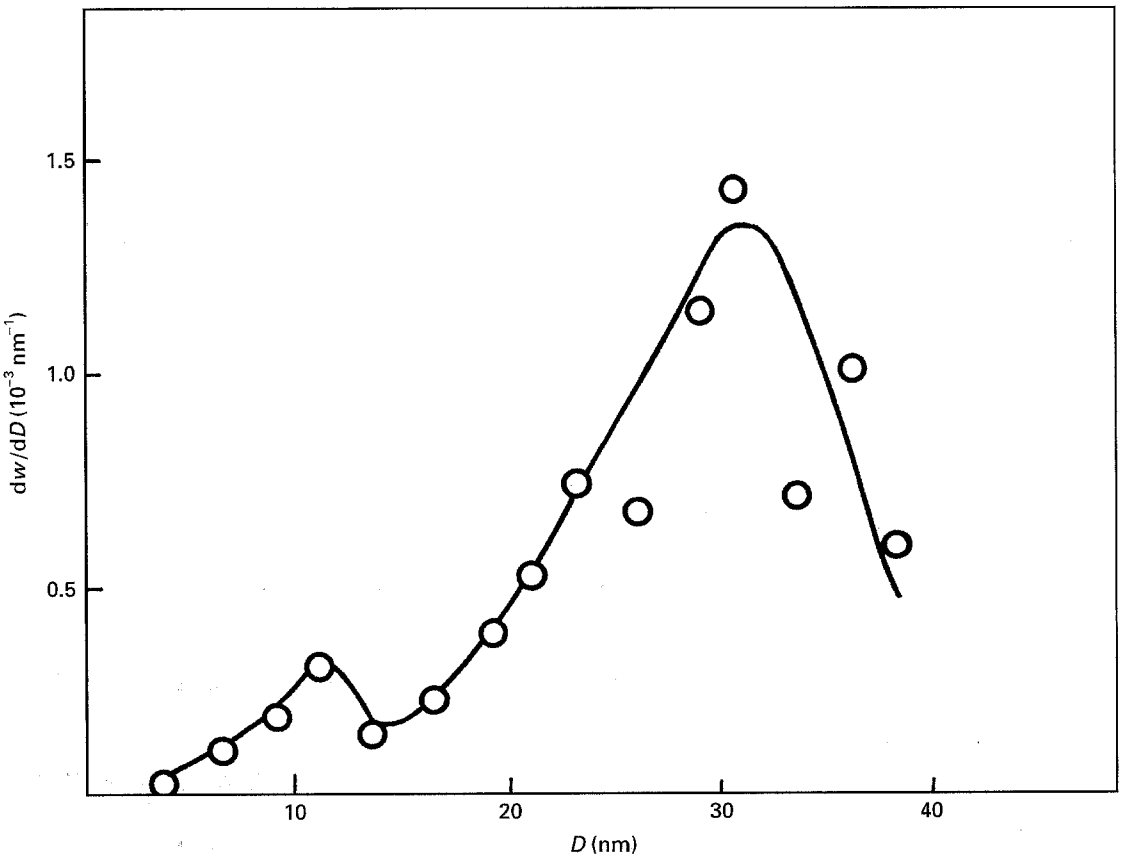

Figure 11 The volume distribution corresponding to Figs 9 and 10.

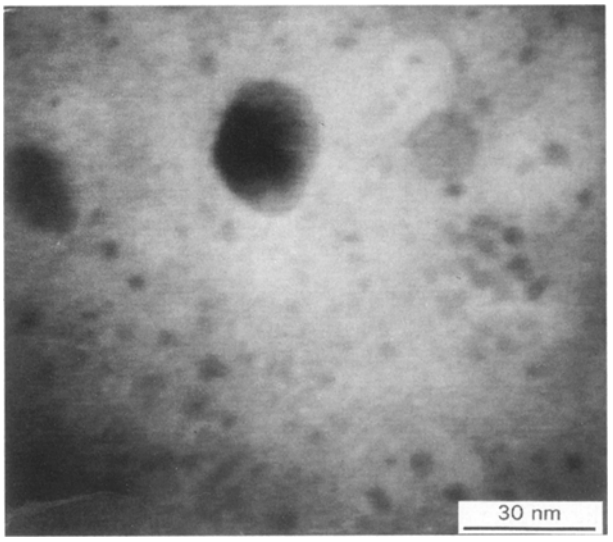

Figure 12 TEM micrograph taken from the sample treated at $T = 480\,°C$, $t = 180$ min, which was thinned by ion sputtering in order to attain electron transparency.

and ultramicrotomy. Fig. 12 shows the result for the sample heat treated at 480 °C for 180 min and prepared by ion sputtering. A few large particles with diameters of about 20–25 nm are surrounded in large numbers by particles with diameters of 2–3 nm. Since it was not certain how the bombardment of the glass with heavy Ar^+ ions influenced the observed size and morphology of the AgCl crystallites, another preparation technique was additionally applied. The TEM investigation of small pieces of the sample, heat treated at 480 °C for 180 min, cut from the bulk material with a diamond knife gave the result presented in Fig. 13. It must be emphasized that with this preparation technique structure changes within the sample can be excluded. Therefore, the result is very remarkable since in this case only a few large particles are observed which are distributed among a large number of very small particles. Indeed, as has been detected by SAXS, the majority of small particles has a diameter of about 2–3 nm. Therefore, the facts obtained by SAXS are fully confirmed by high resolution TEM.

4. Discussion

The experimental SAXS results presented for the treatment at $T = 466\,°C$ lead to the conclusion that for a treatment duration $t \leqslant 60$ min in the system of precipitating AgCl, new particles are formed and grow. This can be derived from the evolution of the volume fraction $w(t)$ and the development of the

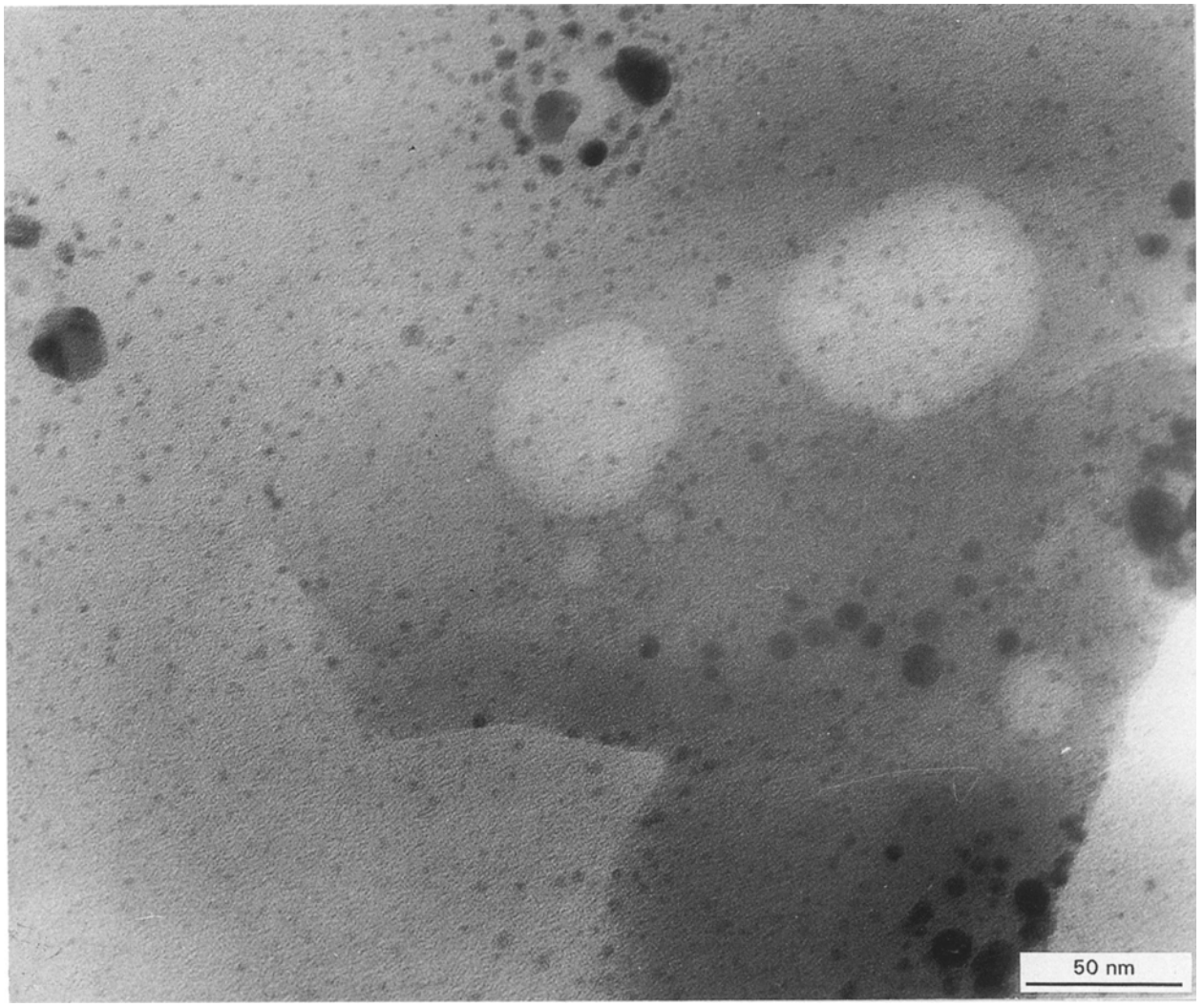

Figure 13 TEM micrograph of the same sample like that in Fig. 12. However, in this case the glass specimen was prepared to an ultrathin platelet by cutting with a diamond knife (ultramicrotomy).

particle number density $N_V(t)$ as well. For $t \leqslant 60$ min w is far below the maximum level for silver halide phase volume (see Fig. 4), and N_V is increasing (see Fig. 5). However, it has to be taken into account that at the very beginning of phase formation the critical diameter of the nuclei formed is smaller than the resolution limit of the SAXS experiment, which amounts to 2 nm under the experimental conditions chosen. Considering the relative supersaturation of the present glass with AgCl $\Delta\mu/(RT) = 1.1 \cdots 1.2$ [13], where R is the molar gas constant and $\Delta\mu$ is the difference between the chemical potentials of the initial homogeneous glass and the final heterogeneous state consisting of completely separated AgCl phase and matrix glass phase, the critical diameter D_{crit} for homogeneous nucleation [28] can be estimated:

$$D_{crit} = 4\sigma V_m/\Delta\mu \qquad (16)$$

The molar volume of the liquid AgCl droplets at the treatment temperature is $V_m = 3 \times 10^{-5}\,m^3\,mol^{-1}$ [29]. The interface tension σ was found to be $8 \times 10^{-2}\,N\,m^{-1}$ [6] and, consequently, D_{crit} is $1.2 \cdots 1.6$ nm for the given treatment temperatures. That means that during the first stage of the heat treatment supercritical particles can not be detected experimentally unless they grow to dimensions larger than the SAXS resolution limit of 2 nm.

For treatment durations $t > 60$ min at 466 °C and $t \geqslant 15$ min at 480 °C the phase separation process shows the typical features of the beginning of Ostwald ripening. The volume fraction of silver chloride particles $w(t)$ remains almost constant close to the maximum value w_{max} (Fig. 4). The particle number density decreases according to $N_V(t) \sim t^{-1}$ (Fig. 5) as has been predicted by the classical LSW theory of diffusion-limited ripening [25, 26]. These findings are consistent with the results shown in Fig. 14, where the validity of the power law

$$\langle D^3\rangle(t) - \langle D^3\rangle(t_0) = U(t - t_0) \qquad (17)$$

which is typical for the mentioned ripening mechanism, is demonstrated by means of the evolution of the size parameter D_1. The constant U depends on the diffusion mobility and the interface tension and, therefore, U is a function of the glass composition and the treatment temperature. t_0 is the starting time for ripening; for example $t_0 = 60$ min for $T = 466$ °C. D_1 is the size parameter that is obtained by the quotient of the third and the fourth moment of the size distribution and, therefore, D_1 represents the first moment of the volume distribution function:

$$D_1 = \frac{\int_0^\infty D^4 dN(D)}{\int_0^\infty D^3 dN(D)} \qquad (18)$$

The size parameter D_1 is approximately equal to the mean diameter of a particle system and it has the advantage that it can be determined with relatively high accuracy from the SAXS curves without applying any transformation procedure [18]. It has been shown elsewhere [30] that the growth law (Equation 17) is valid not only for the mean diameter $\langle D\rangle$ but also for D_1 (with a modified pre-factor U). In Fig. 14 the straight line for all treatment stages in the case of $T = 480$ °C confirms that the ripening process had already started during the first treatment interval of 15 min. In the case of $T = 466$ °C the plot shows that ripening becomes the prevailing growth mechanism

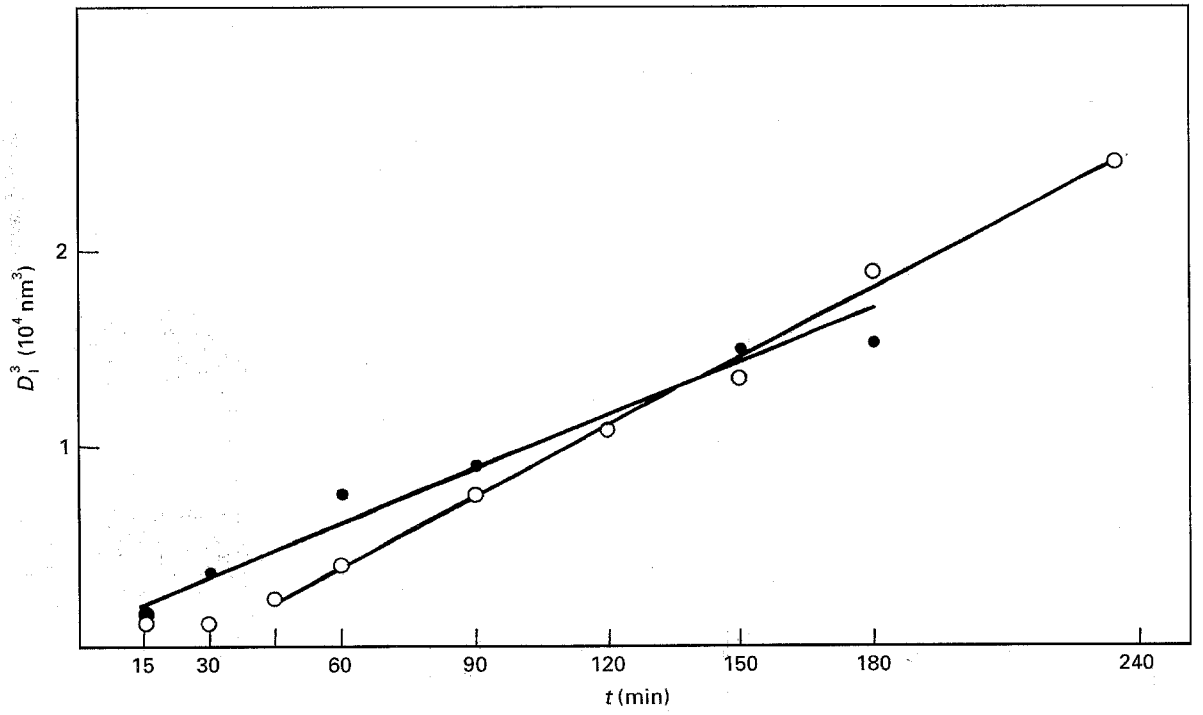

Figure 14 Evolution of the cubed diameter D_1 determined by SAXS during heat treatment. D_1 is the quotient of the third and fourth moment of the size distribution and, therefore, D_1 is the mean diameter of the volume distribution function dw/dD. Key: ● $T = 480$ °C; ○ $T = 466$ °C.

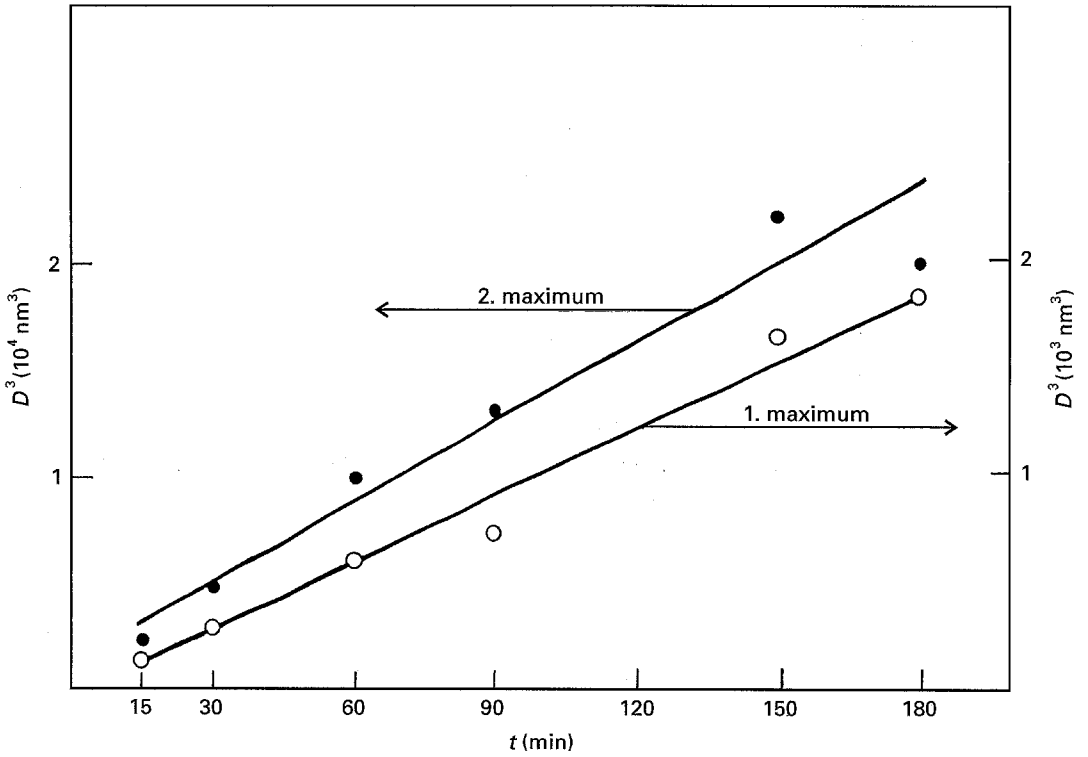

Figure 15 Development of the cubed maximum positions of the small (1) and large (2) crystallites in the volume distributions shown in Fig. 7b, which are obtained from SAXS data.

after 60 min treatment. These conclusions correspond to the results already obtained from Fig. 5.

Obviously, the maxima of both the smaller particles and the larger particles, in the volume distribution functions, shift to larger diameters during the isothermal treatment (Figs. 6b and 7b). This behaviour is further investigated in Fig. 15 by plotting the cubed diameters determined from the maximum positions in the volume distribution functions versus treatment time t. Fig. 15 evidently demonstrates that the mean diameters of the distinct populations of small and large AgCl droplets are growing in the observed stage at the beginning of ripening. It is a very interesting fact that the mean size of the large particles is growing even faster than the mean size of the small clusters (compare the slopes in Fig. 15). Both mean diameters grow according to the power law of diffusion-limited ripening (Equation 17).

These findings are very surprising for ripening which is characterized by a competitive growth that should result in the dissolution of the smallest droplets. Up to now this ripening behaviour of our bimodal size distributions can not be interpreted theoretically. Though, in [13] model computations gave the result that bimodal size distributions with growing mean diameters can be obtained if a predistribution of AgCl crystallites already exists in the initial glass before the isothermal treatment starts. The result in [13], however, was obtained only as an intermediate stage of nucleation and growth, where the population of small clusters grew more rapidly and finally both peaks united.

Another important result that should be discussed in detail is the existence of bimodal-type size distributions which have been proved by the TEM investigations used, applying different resolution conditions and various preparation techniques. This means that these experimental findings, first concluded from SAXS results [9–13], are confirmed by means of the present combination of different methods. For the glass sample treated for 180 min at $T = 480\,^{\circ}C$ the courses of both the size distribution and the volume distribution determined by SAXS are even quantitatively confirmed by the corresponding distributions extracted from TEM micrographs of AgCl precipitates in centrifuged aqueous solutions of the glass (compare Figs 6, 7 and 10, 11). The TEM results of thin glass platelets prepared either with ion sputtering or ultramicrotomy also support these results qualitatively. The micrographs in Figs 12 and 13 show very clearly that the particle ensemble really consists of only a few large AgCl crystallites and a majority of small halide crystallites in the size range of 2–3 nm.

The phenomenon of a bimodal size distribution even in the Ostwald ripening stage can be discussed based on a theoretical model computation which allows the calculation of the expected size distribution under different conditions for a given set of thermodynamic parameters of the glass [13]. The analysis showed that, assuming a growth by attachment of single monomers and non-overlapping diffusion zones of the forming particles, bimodal-type size distributions can only be obtained by homogeneous nucleation and growth, if a size-dependent diffusion coefficient in consequence of elastic strain effects is considered [13].

Additionally, a very interesting feature concerning the spatial arrangement of the AgCl crystallites in the present glass must be mentioned. As can be observed

in Fig. 13 small particles surround the large clusters and the distances between them are very small in relation to the distances between other particles in the system. Up to now an explanation for this "atoll-like" arrangement of the precipitates can not be given by the present theories of nucleation and particle growth.

5. Conclusions

In the present study the results of SAXS investigations according to which the AgCl precipitates in photochromic model glasses and commercial photochromic glasses show size distributions with two significant peaks have been proved using a combination of SAXS and TEM with different preparation techniques. High resolution TEM micrographs obtained from AgCl precipitates centrifuged from aqueous solutions of the water soluble model glass and obtained from thinned glass platelets evidently confirm the bimodality of AgCl crystallite size distributions which have been produced during an isothermal heat treatment of the glass.

The system of silver halide droplets in the glass melt was formed via nucleation and growth. The late stage of growth is characterized by coarsening according to the laws of Ostwald ripening. In the experimentally investigated stage of the beginning of ripening, the populations of both the small and large particles grow according to the power law $\langle D \rangle^3 \sim t$ of diffusion-limited ripening, whereby the mean diameter of the ensemble of large clusters increases more rapidly than the mean diameter of the small crystallites.

In the TEM micrographs taken from samples thinned by ultramicrotomy an "atoll-like" arrangement of small clusters surrounding large particles was observed.

The results of the investigation presented demonstrate that frequently the combination of diffraction methods and electron microscopy is necessary in order to provide a deeper insight into the structure and to obtain additional information which can not be obtained by applying only one single method. In particular, for investigating the kinetics of phase separation on the basis of a series of samples SAXS has the advantage of supplying structure information about particle systems with high statistical certainty. In general the SAXS size parameters are averaged over at least 10^{10} particles. Furthermore, the preparation of glass samples for SAXS experiments is much easier than for TEM investigations. Moreover, the handling of the experiment and the method of calculation for structure parameters is not complicated and allows a fast investigation. This is why SAXS can be complementary to direct structure investigations with TEM and should be used preferentially if the kinetics of phase formation has to be studied for very small particle sizes with high statistical accuracy.

References

1. R. J. ARAUJO, in "Photochromism", edited by G. H. Brown, (Wiley, New York, 1971) Ch. VIII, p. 667.
2. *Idem*, in "Treatise on Materials Sciences and Technology", Vol. 12, "Glass I: Interaction with Electromagnetic Radiation" (Academic Press, New York, San Francisco, London, 1977) p. 91.
3. W. H. ARMISTEAD and S. D. STOOKEY, US Patent DT-AS 1.421.838 (30.12.1960 and 24.11.1961) Corning Glass Works, Corning, New York, USA.
4. *Idem, Science* **144** (1964) 150.
5. S. D. STOOKEY, *Ceram. Ind.* **82** (1964) 97.
6. R. PASCOVA and I. GUTZOW, *Glastechn. Ber.* **56** (1983) 324.
7. *Idem, Phys. Chem. Glasses* **27** (1986) 140.
8. R. PASCOVA, I. GUTZOW and I. TOMOV, *J. Mater. Sci.* **25** (1990) 914.
9. U. LEMBKE, PhD thesis, University of Rostock, Rostock (1986).
10. U. LEMBKE, G. WALTER and W. BLAU, *Studia Biophys.* **112** (1986) 271.
11. U. LEMBKE, W. GÖCKE and W. BLAU, *Rostock. Phys. Manuskr.* **12** (1988) 17.
12. U. LEMBKE and W. GÖCKE, in " Amorphous Structures – Methods and Results", Physical Research, Vol. 12, edited by D. Schulze (Akademie-Verlag, Berlin, 1990) p. 149.
13. J. BARTELS, U. LEMBKE, R. PASCOVA, J. SCHMELZER and I. GUTZOW, *J. Non-Cryst. Solids* **136** (1991) 181.
14. O. KRATKY, G. POROD and Z. SKALA, *Acta Physica Austr.* **13** (1960) 76.
15. A. GUINIER and G. FOURNET, "Small-Angle Scattering of X-rays" (Wiley, New York, and Chapman and Hall, London, 1955).
16. L. A. FEIGIN and D. I. SVERGUN, "Structure Analysis by Small-Angle X-ray and Neutron Scattering" (Plenum Press, New York, 1987).
17. P. W. SCHMIDT, in Summer School on Diffraction Studies on Non-Crystalline Substances, Pecs, Hungary, 1978.
18. G. WALTER, R. KRANOLD, TH. GERBER, J. BALDRIAN and M. STEINHART, *J. Appl. Cryst.* **18** (1985) 205.
19. G. POROD, *Kolloid-Zeitschrift* **124** (1951) 83.
20. C. V. DAVIES and X. NANCOLAS, *Trans. Faraday Soc.* **51** (1955) 823.
21. O. BECKER, O. ANDERSON and H. BACH, Beitr. Elektronenmikroskop. Direktabb. Oberfl. **22** (1989) 341.
22. F. ZÖRGIEBEL, H. P. ZEINDL and G. HAASE, *Ultramicroscopy* **16** (1985) 115.
23. T. F. MALIS and D. STEELE, *Mater. Res. Soc. Symp. Proc.* **199** (1990) 3.
24. O. BECKER and K. BANGE, *Ultramicroscopy* **52** (1993) 73.
25. I. M. LIFSHITZ and V. V. SLYOZOV, *J. Phys. Chem. Solids* **19** (1961) 35.
26. C. WAGNER, *Z. Elektrochem. Ber. Bunsenges. Phys. Chem.* **65** (1961) 581.
27. S. TOSHEV and I. GUTZOW, *Phys. Status Solidi* **24** (1967) 349.
28. M. VOLMER, "Kinetik der Phasenbildung" (Steinkopff, Dresden, 1939).
29. Gmelins Handbuch der anorganischen Chemie, Silber, Syst.-Nr. 61, Teil B1, 8. Auflage (Verlag Chemie-GmbH. Weinheim/Bergstrasse, 1971) p. 330.
30. J. MÖLLER, K. KRANOLD, J. SCHMELZER and U. LEMBKE, *J. Appl. Cryst.*, **28** (1995) 553.

Received 12 May
and accepted 1 December 1995